Research Article

Shannon C. Knight, Bret A. Unger, and Kurt W. Kolasinski*

Crystallographically Defined Silicon Macropore Membranes

https://doi.org/10.1515/oms-2018-0004
Received Jul 17, 2018; accepted Aug 27, 2018

Abstract: Laser ablation with nanosecond-pulsed Nd:YAG laser irradiation combined with anisotropic alkaline etching of Si wafers creates 4–20 μm macropores that extend all the way through the wafer. The walls of these macropores are crystallographically defined by the interaction of the anisotropy of the etchant with the orientation of the single-crystal silicon substrate: rectangular/octagonal on Si(001), parallelepiped on Si(110), triangular/hexagonal on Si(111). Laser ablation can create pillars with peak-to-valley heights of over 100 μm. However, with nanosecond-pulsed irradiation at 532 nm, the majority of this height is created by growth above the original plane of the substrate whereas for 355 nm irradiation, the majority of the height is located below the initial plane of the substrate. Repeated cycles of ablation and alkaline etching are required for membrane formation. Therefore, irradiating with 355 nm maintained better the crystallographically defined nature of the through-pores whereas irradiation at 532 nm led to more significant pore merging and less regularity in the macropore shapes. Texturing of the substrates with alkaline-etching induced pyramids or near-field modulation of the laser intensity by diffraction off of a grid or grating is used to modulate the growth of ablation pillars and the resulting macropores. Texturing causes the macropores to be more uniform and significantly improves the yield of macropores. The size range of these macropores may make them useful in single-cell biological studies.

***Corresponding Author: Kurt W. Kolasinski:** Department of Chemistry, West Chester University, West Chester, PA 19380-2115 United States of America; Email: kkolasinski@wcupa.edu
Shannon C. Knight: Renaissance Academy Charter School, 400 Franklin Ave., Phoenixville, PA 19460 United States of America
Bret A. Unger: Department of Chemistry, University of California Berkeley, Berkeley, CA 94720-0001 United States of America

1 Introduction

Alkaline etching of Si in aqueous KOH, NaOH or tetramethyl ammonium hydroxide (TMAH) solutions is highly anisotropic and has been used to create three-dimensional microstructures as well as electromechanical and micromechanical devices including X-ray masks, optical waveguides, high-resolution patterns, nozzles, and microtools [1]. Surface texturization by alkaline etching of Si is a standard procedure to increase the efficiency of photovoltaic cells by decreasing their reflectivity [2–6]. It has been used to create a membrane with a single pore [7]. Plasma etching with patterned masks, laser drilling (*i.e.* laser ablation) with serial irradiation of individual spots and combinations of the two have been used to render polymer membranes porous [8, 9] that are suitable for aerosolized delivery of therapeutic or diagnostic agents. Laser drilling in air or water [10] is used to make through-pores, which has the advantage of being able to reproducibly create microscale through-pores but has the disadvantage of being a serial process. Photolithographic patterning, chemical vapor deposition (CVD) and sacrificial oxide removal have been used to create Si membrane filters in which the pores have dimensions in the tens of nanometer range [11, 12]. Filters in this size range can be used for virus removal and immunoisolation. Saito and Kimura [13] combined patterned laser irradiation with alkaline etching of Si to produce crystallographically defined pits. Khuat *et al.* [14] have used 150 fs pulses of 800 nm laser light focused to 3.2 μm followed by etching in concentrated HF + HNO_3 solutions to etch through-pores in SiC in a serial fashion.

Cellular development responds in a complex manner to an array of chemical and geometrical cues [15–19]. Using both coatings and micro-patterning, control of biochemistry at the cell-biomaterial interface represents one strategy to improve, *e.g.*, endothelial healing. Micropatterned substrates serve to control cell shape, cytoskeletal structure, proliferation rate, and apoptosis by limiting the available geometric area to which cells can adhere [20–22]. Non-symmetric shapes in the micro-pattern promote directional cell motility [23] that may be useful for promoting wound healing responses in terms of endothelial area coverage. Micro-patterned silicon arrays represent a single-cell reaction platform that can be easily functionalized with amines [24–27] for the binding of epitopes to promote adhesion and differentiation. Incorporating micro-patterned silicon into a membrane would allow for flow/wash assays where the surfaces are functionalized with single stranded DNA (ssDNA). Such membranes could be exposed to ssDNA-epitope complexes that could be washed away and replaced, similar to the approach of, *e.g.*, Freeman *et al.* [28].

Silicon exposed to laser ablation changes from a shiny gray mirror to a black surface with little to no reflectivity [29, 30]. The blackest surfaces are obtained from a regular array of sharp pillars. The highly inclined sides of the pillars are naturally reflective because reflectivity increases with increasing angle of incidence. As the irradiation proceeds, hot valleys with (relatively) cold tips are created, which leads not only to a transfer of material from the valleys to the tips, but also growth of the tips above the initial plane of the substrate. The proportion of Si deposited out of the ablation plume onto the target can be controlled to some extent by controlling the pressure and chemical composition of the gas above the target during ablation. Pillars produced by irradiation with nanosecond pulsed lasers, *e.g.* Nd:YAG or excimer lasers, in the presence of SF_6 or Ar are solid with crystalline cores surrounded by deep valleys with a semi-regular spacing [31]. The crystallinity of the pillars and the substrate below are important, and we use them here as the basis for the production of macropores, which are created by anisotropic etching in aqueous KOH solutions [32].

The etch rate of Si in KOH(aq) is strongly dependent on the surface crystallography because of the different surface atom co-ordinations that occur on different planes [33, 34]. The resulting etch rates are highly anisotropic, *i.e.* different for different surface planes (*hkl*), because of the formation of a sterically constrained pentavalent transition state [35, 36] coupled to the crystallographically defined manner in which different surface planes can accommodate this constrained structure.

Si pillars are first sharpened by alkaline etching and then give way to the emergence of macropores [31]. During etching the pillars anchor the sidewalls that eventually define macropores. Macropore shapes are dependent on crystallographic properties of the substrate as has been shown on both Si(001) and Si(111) substrates [32].

In this work, we extend previous work to Si(110) substrates and demonstrate the formation of regular arrays of parallelepiped macropores. We then explore the formation of macropore membranes in which the macropores extend completely through the wafer. An optimized procedure is reported for membrane production. Nanosecond pulsed Nd:YAG irradiation at 355 nm is preferred to 532 nm irradiation. Both sides of the wafer are ablated then etched in KOH(aq) to produce the membranes.

2 Experimental

Silicon (001), (110), and (111) wafers used for this study were obtained from University Wafer: Si(001) prime grade, 0–100 Ω cm, B doped, p type; Si(110) prime grade 1–10 Ω cm, B doped, p type; Si(111) mechanical grade, unspecified doping. Laser ablation was performed using a SpectraPhysics Indi Nd:YAG laser producing 135 mJ at 355 nm or 180 mJ at 532 nm in 6 ns pulses and a 20 Hz repetition rate. Parameters were set for ablation as follows: An antireflection-coated 50 cm plano-convex lens placed 35.5 cm from the substrate, a wavelength of 532 nm, a scanning rate of 0.04–0.12 mm s^{-1}, a pressure of 0.7–1.5 kPa of flowing 5% SF_6diluted in N_2 (Praxair) and a pass separation of 1.5 mm such that overlapping laser irradiation occurs from one pass to the next. The corresponding fluence and spots size (diameter) are 2.9 J cm^{--2} and 2.8 mm. We also performed the experiment using a 50 cm plano-convex lens placed at 33 cm from the substrate, a wavelength of 355 nm, a scanning rate of 0.04–0.12 mm s^{-1}, a pressure of 0.7–1.5 kPa of flowing SF_6 in N_2, and a pass separation of 1.25 mm. The corresponding fluence and spots size are 1.7 J cm^{--2} and 2.2 mm. The wafer is tilted slightly upward (~10°) to avoid damage to the antireflection-coated chamber window from back-reflections. Low pressure was used to allow expansion of the laser plume and limit deposition onto the substrate and enhance the depth of the valleys. The number of laser shots to which any area of the sample is exposed is controlled by changing the rate at which the target is scanned across the fixed laser beam spot, and corresponds to 400–1600 shots over the scan rate range of 0.04–0.12 mm s^{-1}. If the scanning rate is too fast, the pillars are shallower and eventually do not form fully. This leads to poor sidewall anchoring such that they do not withstand etching sufficiently to form well-defined macropores. Because the spot size is > 2 mm and areas on the order of 1 cm^2 are generally irradiated re-alignment between cycles of ablation is not critical and was only controlled to within a few millimeters.

Anisotropic etching was performed using either 40% KOH (w/w) in water with a constant temperature of 80°C or 12.5% KOH + 2% isopropyl alcohol (IPA) in water at 70°C. In 40% KOH, the etch rate of Si(001) is ~35 μm h^{-1} and is less than that of Si(110), which is ~40 μm h^{-1} [33]. In 12.5% KOH + 2% IPA, the etch rate of Si(001) drops to ~20 μm h^{-1} but exceeds that of Si(110), which is only ~7 μm h^{-1}. ACS reagent grade KOH from VWR was used.

An FEI Quanta 400 ESEM was used to generate secondary electron (SE) scanning electron micrographs (SEM) and probe the substrate structure. To make membranes, the sample was exposed to repeated ablation/KOH etching cycles. It was found that ablation with both 532 nm and 355 nm irradiation created a pillar tip-to-valley distance that could approach (in the case of 355 nm irradiation) or exceed 100 μm (for 532 nm irradiation). At 532 nm, the pillars grew 60–80 μm above the surface, whereas with the 355 nm, the pillars grew 10–25 μm above the surface and then extended ~50 μm or more into the wafer.

To form membranes, the sample was ablated on both sides of the wafer prior to KOH etching. We call this an ablation-etching cycle. Membranes were formed in 300 μm thick Si(100) substrates after three ablation/etching cycles for 532 nm irradiation whereas some through pores were already observed after only two cycles for 355 nm irradiation. A significantly higher proportion of through-pores is observed if the scan direction of ablation is rotated by 90° between successive ablation-etching cycles.

3 Results and discussions

3.1 Macropore formation

Ablation in Ar and N_2 enhances growth of the pillars above the initial plane of the substrate, which is not advantageous to membrane formation. Ablation in 5% SF_6/N_2 enhances Si volatilization and the formation of deeper valleys as compared to ablation in the same pressure of either Ar or pure N_2. Switching to 5% SF_6/N_2 also created sharper, more uniform pillars that can be formed over a broader range of ablation conditions. To obtain the same depth and improved sharpness, the scan rate can be increased from 0.02 mm s^{-1} for ablation in Ar or N_2 to 0.04 mm s^{-1} for ablation in 5% SF_6/N_2.

Macropore shapes are dependent on crystallographic properties of the substrate. As exhibited in Figure 1(a), Si(100) is etched such that the resulting macropores are rectangular with vertical walls and an inverted pyramidal bottom (as confirmed by cross sectional imaging [32]). Rectangular macropores are exclusively observed on Si(100) when 40% KOH is used for etching. However, as will be shown below, when etching with 12.5% KOH + 2% IPA, octagonal through-pores have occasionally been observed. As observed previously [32, 37], Si(111) has a transition from hexagonal to triangular macropores that are aligned in one direction when etching with 40% KOH or tetramethyl ammonium hydroxide (TMAH). However as shown in Figure 1(b), while etching in 12.5% KOH + 2% IPA eventually leads to equivalent triangular pores, the shapes assumed prior to this are only infrequently hexagonal and usually more irregular. The pore walls that are formed are highly inclined and stepped. Macropore formation from alkaline etching of laser ablation pillars on Si(110) has not previously been characterized. Figure 1(c) demonstrates that Si(110) exhibits parallelepiped macropores with a combination of vertical and inclined walls.

3.2 Membrane formation

Membrane formation requires dual optimization of ablation and KOH etching. KOH etching at first sharpens the pillars then leads to the formation of crystallographically defined macropores. However, overetching leads to the loss of crystallographically defined features before macropores have etched through. Ablation of crystallographically defined macropores leads to the re-formation of sharp pillars, which can again be KOH etched. A combination of ablation on both sides of the wafer and re-ablation of KOH etched macropores is required for membrane formation when pillars are formed randomly. We have found that macropores propagate best on Si(001); therefore, we concentrated our membrane formation efforts on (001) substrates.

Using 300 μm thick wafers, we found that three cycles of ablation on both sides of the wafer and KOH etching were required to form membranes with through-pores when using 532 nm irradiation. During the third cycle pore merging becomes commonplace, the outer surface becomes extremely irregular, and the macropores begin to lose their crystallographic definition. However, when using 355 nm irradiation, only two cycles of two-sided ablation and KOH etching were required. This led to significantly better shape retention as can be seen in Figure 2. Macropore formation was confirmed by visible light transmission. Nonetheless, Figure 2 demonstrates that there is an irregular pattern of macropores that propagated and others that have ceased to propagate. Very few of the macropores actually propagate all the way through the substrate. The cross-section in Figure 2(b) demonstrates that macropores well over 150 μm in length would be frequently formed if better alignment of macropores could be achieved. Better alignment of the pores with respect to their neighbors and uniformity of depth would also reduce

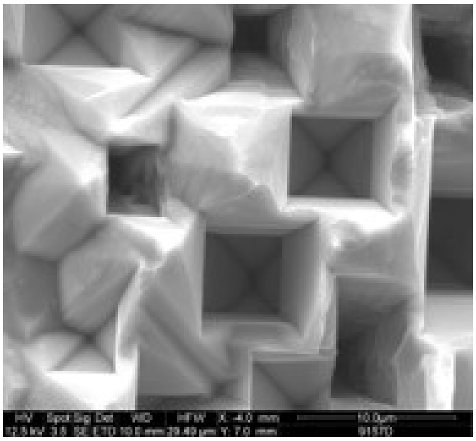

(a) Si(100)

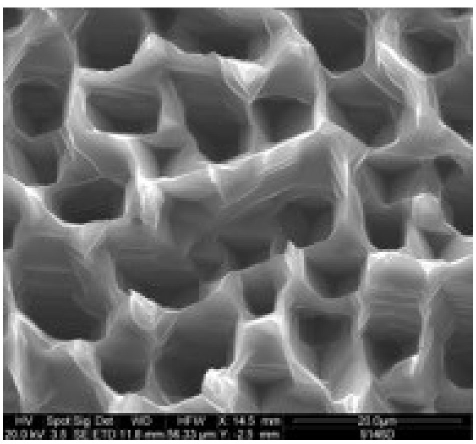

(b) Si(111)

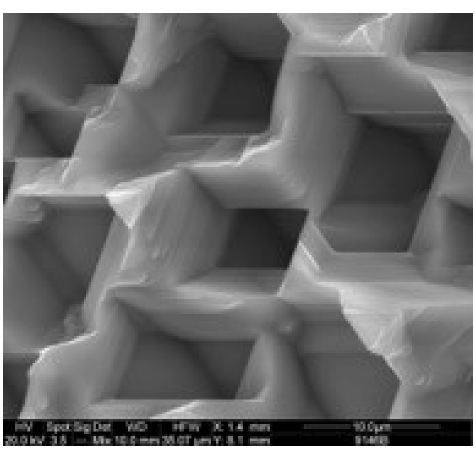

(c) Si(110)

Figure 1: Crystallographically defined macropores etched with 12.5% KOH + 2% IPA. (a) Si(100) produces rectangular macropores. Much less frequently octagonal macropores are also observed but only for through-pores. (b) Si(111) first produces irregular macropores that eventually convert to triangular macropores. (c) Si(110) produces parallelepiped pores.

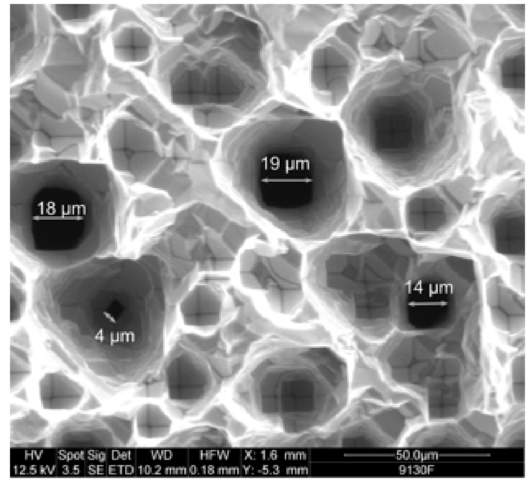

(a)

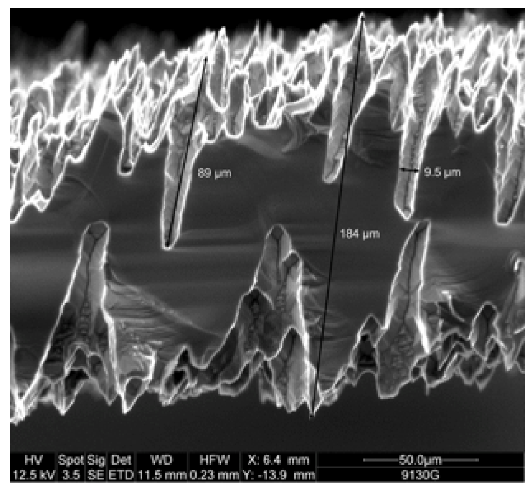

(b)

Figure 2: Through-pores formed after two etching-ablation cycles at 355 nm on Si(100) using 40% KOH. (a) Four neighboring macropores that are etched all the way through the substrate. The 4–µm pore is rotated by 45° compared to the 14–19 µm pores. (b) Cross-sectional image of a sample containing through-pores as well as macropores that have not formed through-pores because of mis-alignment.

the amount of pore merging. However, the random alignment of pillars and, therefore, macropores on the top and bottom surfaces translates into only the occasional "super-propagating" pore making it all the way through the substrate.

Riedel *et al.* [38] and Mills and Kolasinski [31, 39] have described several methods of producing ordered ablation pillars. These involve using diffraction to modulate the laser intensity profile, which in turn modulates the formation of pillars in a regular fashion. Riedel *et al.* used diffraction off the side of a wire to align rows of pillars along the wire axis. The method of Mills utilizes a ruled grating to align the pillars both in and between the rulings. Here we introduce a hybrid of these methods. First the Si wafer was annealed in air at 1000°C for 2 hours. This produces an oxide layer that is blue in appearance due to optical interference. Then an Al grid was affixed to the surface of the substrate to act as an ablation mask. Ablation pillars form in the exposed area. The results shown in Figure 3 demonstrate ordering of several rows of pillars and the macropores developed upon etching. The ablation grid was composed of ~250 μm diameter wires spaced rectangularly in a 1 mm × 1.25 mm pitch. The grid is not substantially ablated and can be reused multiple times.

SiO_2 remaining in the shadowed regions that were beneath the grid wires acts as a mask for KOH etching. The masked regions retain their initial thickness after the first ablation-etch cycle. This enhances the rigidity of the membrane and also aids in maintaining alignment of the macropores that develop after the second ablation-etch cycle.

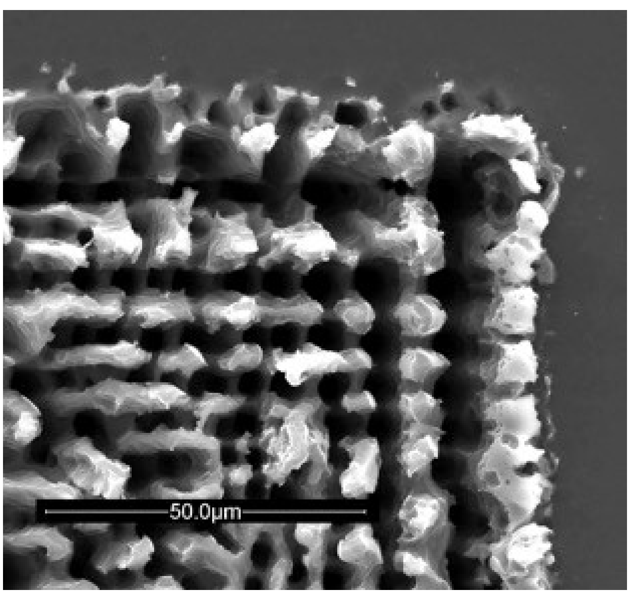

Figure 3: SE-SEM image of an ablated sample that was lightly (2.5 min) etched in 40% KOH. A grid was used as an ablation mask on a surface-oxidized Si wafer. Ablation through the grid led to ordering of the pillars and subsequent macropores that were formed during KOH etching. The oxide acts as an etch mask; therefore, the substrate below the grid wires was neither thinned nor subjected to pillar/macropore formation.

Both ruled gratings and grid ablation with oxide etch masks led to enhanced formation of through-pores. This was especially pronounced in the rules or close to the grid lines. However, unless careful alignment of the ruled gratings or grids on both the top and bottom surfaces of the substrate was performed, the enhancement was still somewhat haphazard.

Finally we explored one other technique to influence the formation of the pillars. Texturing of Si solar cells to reduce visible light reflectivity is routinely performed with alkaline etching [6]. This creates a semi-regular array of pyramids on the Si substrates, which are responsible for the reduction in reflectivity, as shown in Figure 4(a).

Laser ablation of a pyramid-covered Si surface led to facile pillar formation, as shown in Figure 4(b). Particularly important for membrane formation, an initially pyramid-covered surface enhanced the production of extremely narrow and deep crevices between ablation pillars. We also observed that etching with 12.5% KOH + 2% IPA can be used to completely remove ablation pillars and their replacement by a pyramid-covered surface. This led us to a much-improved method for the formation of membranes with an appreciable coverage of microscale through-pores across the breadth of the ablated area. This protocol is presented schematically in Figure 5.

Step 1 is to anneal the Si(100) substrate at 1000°C for 2 h. This creates a thick, uniform SiO_2 layer. This layer does not hinder the formation of laser ablation pillars but it does create a mask that can withstand etching in 12.5% KOH + 2% IPA at 70°C for > 2h.

Step 2 is to ablate the sample with 355 nm light in 1 kPa of 5% SF_6 in N_2. A scan rate of 0.04 mm s^{-1} at a fluence of ~1.7 J cm^{--2} creates deep and regular ablation pillars.

Step 3 is to etch at 70°C in 12.5% KOH + 2% IPA. This etchant is fastest in the [001]-direction, slower in the [110]- and slowest in the [111]-direction. After 30 min the pillars and almost all macropores have been removed and are replaced by pyramids. The sample can be thinned and more uniformly covered with pyramids by etching for longer times. As shown in the first inset for Step 3, etching only occurred in the ablated region. Therefore, either by ablation through a grid or by direct laser writing, a pattern of pillars can be formed which is then selectively removed by KOH + IPA etching to thin the sample and form pyramids only in the previously irradiated area. This allows for the production of a patterned membrane of through-pores by the next two steps. Samples thinned and pyramid-covered by etching for 90–120 min were found to produce high coverages of through-pores after the next two steps.

Step 4 is to ablate the pyramid-covered surface with direction of rastering orthogonal to the original laser raster direction. The same parameters as in Step 2 were used for ablation in Step 4.

Step 5 is to complete the second ablation-etch cycle by etching at 70 °C in 12.5% KOH + 2% IPA for 5–10 min.

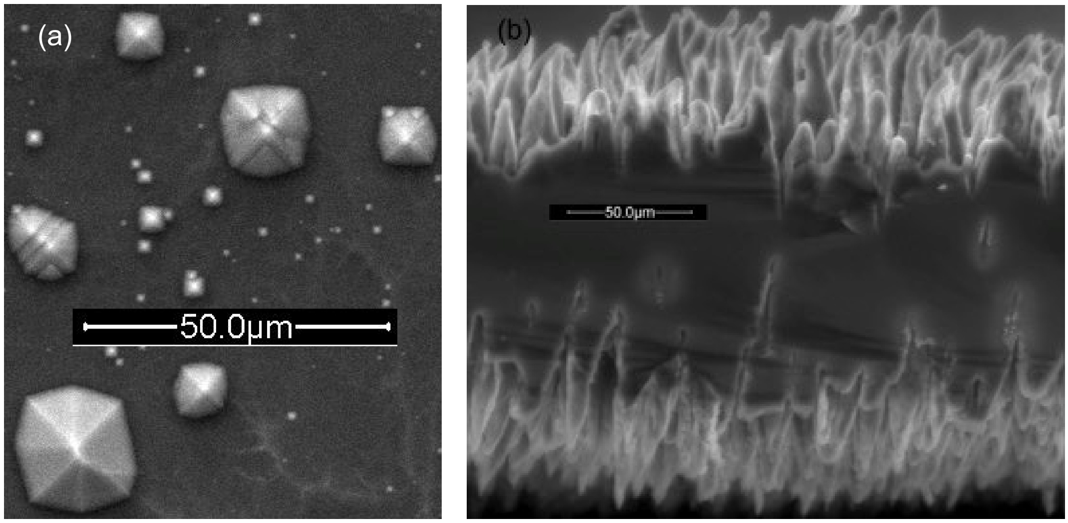

Figure 4: (a) Plan-view SE-SEM image of pyramids created by etching Si in 12.5% KOH + 2% IPA. (b) Cross-sectional SE-SEM image of laser ablation pillars formed by irradiation of a pyramid-covered surface. An initially pyramid-covered surface enhances the production of extremely narrow and deep crevices between ablation pillars.

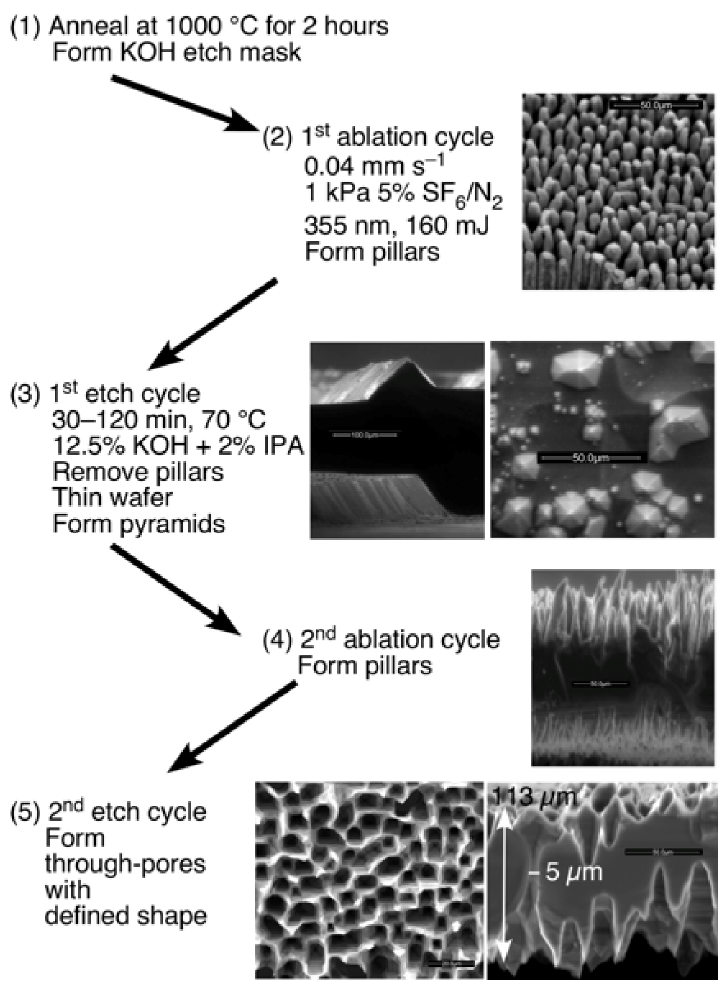

Figure 5: Schematic depiction of the steps of an optimized Si membrane formation protocol.

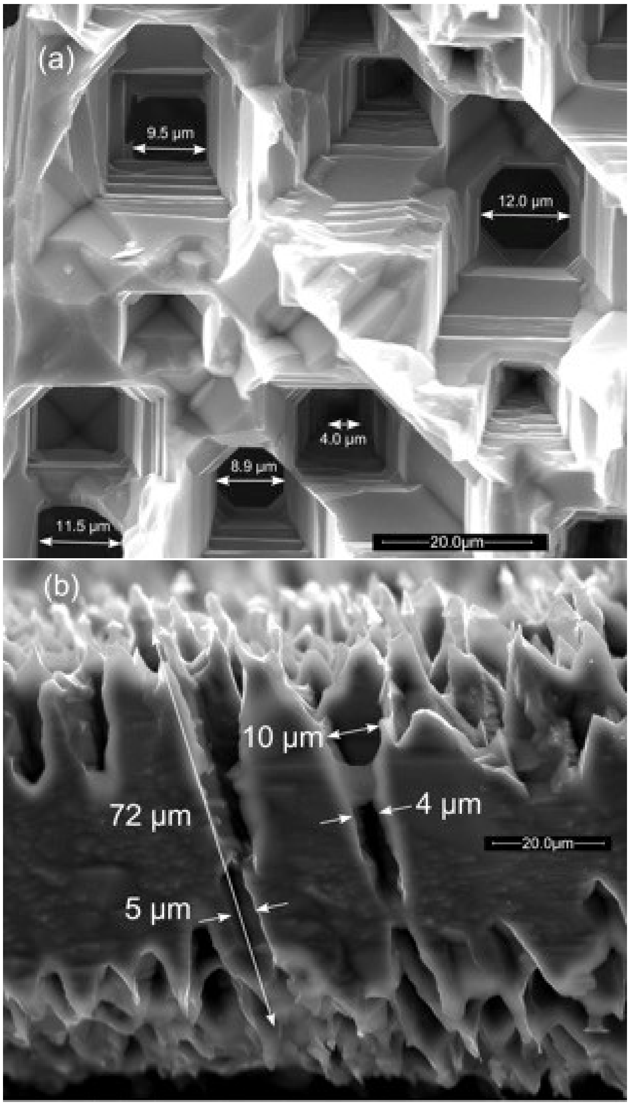

Figure 6: (a) Plan-view SE-SEM image of a region that exhibits approximately 10% coverage of through-pores after application of the ablation-etch protocol outlined in Figure 5. Through-pores ranging from 4 to 12 µm in width are observed. Both rectangular and octagonal through-pores are found. (b) Cross-sectional SE-SEM image of a Si membrane formed from the same protocol.

The results of the optimized protocol are exhibited in the inset of Step 5 in Figure 5 as well as in Figure 6. The existence of through-pores is confirmed not only by plan-view and cross-sectional imaging, but also by the observation of the transmission of red light from a HeNe laser. Macropores with a minimum width of 4–12 µm are revealed in the image in Figure 6(a). This is consistent with the cross-sectional image in Figure 6(b). The cross-sectional image reveals what appear to be two different types of through-pores. The one to the right proceeds from top to bottom with a clear aperture. The one on the left appears to be formed from the joining of two macropores that were slightly misaligned. This raises the possibility that some pores may not have direct line-of-site from front to back of the substrate.

A reproducible non-serial method of making patterned membranes in silicon containing crystallographically-defined rectangular and octagonal through-pores with widths in the range of 4–12 µm and membrane thicknesses in excess of 100 µm has been demonstrated. The optimized five-step protocol involves (1) annealing of a Si(100) substrate, (2) laser ablation, (3) anisotropic etching in KOH(aq) + isopropyl alcohol, (4) laser ablation and (5) anisotropic etching in KOH(aq) + isopropyl alcohol. The protocol can be used to produce membranes with arbitrarily large areas in any pattern that can be defined by a laser ablation mask or direct writing during rastering of the laser beam. Further processing of these membranes with stain etching [40], as shown in Figure 7, or regenerative electroless etching [41] creates membranes with high-surface area, nanoporous (3–4 nm) films that exhibits brilliant visible photoluminescence.

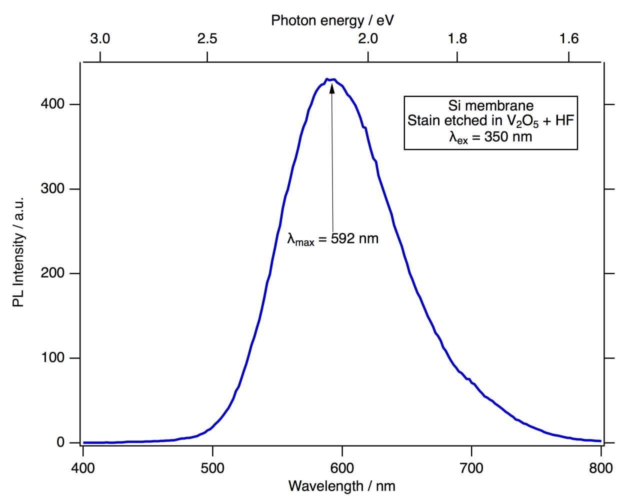

Figure 7: Photoluminescence spectrum obtained from a Si membrane with through-pores that was stain etched for 60 s in 0.12 M V_2O_5 dissolved in concentrated HF(aq).

Acknowledgement: Funding provided by West Chester University and the resources of the Center for Microanalysis and Imaging Research and Training (CMIRT).

References

[1] E. Bassous, *Fabrication of novel three-dimensional microsctructures by the anisotropic etching of (100) and (110) silicon*. IEEE

Trans. Electron Devices 1978, 25, 1178-1185.

[2] P. Papet, O. Nichiporuk, A. Kaminski, Y. Rozier, J. Kraiem, J.-F. Lelievre, A. Chaumartin, A. Fave, M. Lemiti, *Pyramidal texturing of silicon solar cell with TMAH chemical anisotropic etching*. Sol. Energy Mater. 2006, 90, 2319-2328.

[3] F. Llopis, I. Tobías, *Influence of texture feature size on the optical performance of silicon solar cells*. Prog. Photovoltaics 2005, 13, 27-36.

[4] Z. Xi, D. Yang, W. Dan, C. Jun, X. Li, *Texturization of cast multicrystalline silicon for solar cells*. Semicond. Sci. Technol. 2004, 19, 485-489.

[5] J. D. Hylton, A. R. Burgers, W. C. Sinke, *Alkaline etching for reflectance reduction in multicrystalline silicon solar cells*. J. Electrochem. Soc. 2004, 151, G408-G427.

[6] É. Vázsonyi, K. De Clercq, R. Einhaus, E. Van Kerschaver, K. Said, J. Poortmans, J. Szlufcik, J. Nijs, *Improved anisotropic etching process for industrial texturing of silicon solar cells*. Sol. Energy Mater. 1999, 57, 179-188.

[7] E. Bassous, J. M. Blum, K. K. Chan, A. C. Lamberti, C. Lapadula, I. Lovas, A. D. Wilson, *Monolithic silicon membrane device fabrication process*. Patent No. US 4,978,421 (1990).

[8] R. S. Patel, S. Srinivasan, *Reactive ion etching method of fabricating nozzles for aerosolized delivery of therapeutic or diagnositic agents*. Patent No. US 6,295,986 B1 (2001).

[9] Patel, R. S., Srinivasan, S., Pon, R. M., Schuster, J. A., & Gonda, I., *Method of fabricating porous membrane with unique pore structure for aerosolived drug delivery*. Patent No. US 6,551,542 B1 (2003).

[10] Wee, L. M., Ng, E. Y. K., Prathama, A. H., & Zheng, H., *Micromachining of silicon wafer in air and under water*. Optics & Laser Technology 43, 2011, 62-71.

[11] Kittilsland, G., Stemme, G., & Nordén, B., *A sub-micron particle filter in silicon*. Sens. Actuators A 23, 1990, 904-907.

[12] Chu, W.-H., Chin, R., Huen, T., & Ferrari, M., *Silicon membrane nanofilters from sacrificial oxide removal*. J. Microelectromech. Sys. 8, 1999, 34-42.

[13] Saito, M. & Kimura, S., *Polygonal pits on silicon surfaces that are created by laser-assisted chemical etching*. AIP Advances 7, 2017, 025018.

[14] Khuat, V., Ma, Y., Si, J., Chen, T., Chen, F., & Hou, X., *Fabrication of through holes in silicon carbide using femtosecond laser irradiation and acid etching*. Appl. Surf. Sci. 289, 2014, 529-532.

[15] Zawislak, J. P., Kolasinski, K. W., & Helmke, B. P., *Development of endothelial cells on pillar-covered silicon*. Phys. Status Solidi A 206, 2009, 1356-1360.

[16] Choudhary, S., Haberstroh, K. M., & Webster, T. J., *Enhanced functions of vascular cells on nanostructured Ti for improved stent applications*. Tissue Eng. 13, 2007, 1421-1430.

[17] Caves, J. M., & Chaikof, E. L., *The evolving impact of microfabrication and nanotechnology on stent design*. Journal of Vascular Surgery 44, 2006, 1363-1368.

[18] Choudhary, S., Haberstroh, K. M., & Webster, T. J., *Enhanced Functions of Vascular Cells on Nanostructured Ti for Improved Stent Applications*. Tissue Engineering 13, 2007, 1421-1430.

[19] Mott, R. E. & Helmke, B. P., *Mapping the dynamics of shear stress-induced structural changes in endothelial cells*. American Journal of Physiology-Cell Physiology 293, 2007, C1616-C1626.

[20] Ishizaki, T., Saito, N., & Takai, O., *Correlation of Cell Adhesive Behaviors on Superhydrophobic, Superhydrophilic, and Micropatterned Superhydrophobic/Superhydrophilic Surfaces to Their Surface Chemistry*. Langmuir 26, 2010, 8147-8154.

[21] Chen, C. S., Mrksich, M., Huang, S., Whitesides, G. M., & Ingber, D. E, *Geometric Control of Cell Life and Death*. Science 276, 1997, 1425-1428.

[22] Dalby, M. J., Childs, S., Riehle, M. O., Johnstone, H. J. H., Affrossman, S., Curtis, A. S. G., *Fibroblast reaction to island topography: changes in cytoskeleton and morphology with time*. Biomaterials 24, 2003, 927-935.

[23] Jiang, X., Bruzewicz, D. A., Wong, A. P., Piel, M., Whitesides, G. M. *Directing cell migration with asymmetric micropatterns*. Proc. Natl. Acad. Sci. U. S. A. 102, 2005, 975-978.

[24] Ruizendaal, L., Bhattacharjee, S., Pournazari, K., Rosso-Vasic, M., de Haan, L. H. J., Alink, G. M., et al. *Synthesis and cytotoxicity of silicon nanoparticles with covalently attached organic monolayers*, Nanotoxicology 3, 2009, 339-347.

[25] Jarvis, K. L., Barnes, T. J., & Prestidge, C. A., *Surface chemistry of porous silicon and implications for drug encapsulation and delivery applications*. Adv. Colloid Interface Sci. 175, 2012, 25-38.

[26] Li, Y., Calder, S., Yaffe, O., Cahen, D., Haick, H., Kronik, L., et al., *Hybrids of Organic Molecules and Flat, Oxide-Free Silicon: High-Density Monolayers, Electronic Properties, and Functionalization*. Langmuir 28, 2012, 9920-9929.

[27] Sweetman, M. J., Ronci, M., Ghaemi, S. R., Craig, J. E., & Voelcker, N. H., *Porous Silicon Films Micropatterned with Bioelements as Supports for Mammalian Cells*. Adv. Func. Mater. 22, 2012, 1158-1166.

[28] Freeman, R., Stephanopoulos, N., Álvarez, Z., Lewis, J. A., Sur, S., Serrano, C. M., et al. *Instructing cells with programmable peptide DNA hybrids*. Nature Communications 8, 2017, 15982.

[29] Wu, C., Crouch, C. H., Zhao, L., Carey, J. E., Younkin, R., Levinson, J. A., et al., *Near-unity below-band-gap absorption by microstructured silicon*. Appl. Phys. Lett. 2001, 78, 1850-1852.

[30] Vorobyev, A. Y. & Guo, C. L., *Direct femtosecond laser surface nano/microstructuring and its applications*. Laser & Photonics Reviews 7, 2013, 7, 385-407.

[31] Mills, D. & Kolasinski, K. W., *A Non-lithographic method to form ordered arrays of silicon pillars and macropores*. J. Phys. D: Appl. Phys. 38, 2005, 632-636.

[32] Dudley, M. E. & Kolasinski, K. W., *Wet Etching of Pillar Covered Silicon Surface: Formation of Crystallographically Defined Macropores*, J. Electrochem. Soc. 155, 2008, H164-H171.

[33] Wind, R. A. & Hines, M. A., *Macroscopic etch anisotropies and microscopic reaction mechanisms: a micromachined structure for the rapid assay of etchant anisotropy*. Surf. Sci. 460, 2000, 21-38.

[34] Zubel, I., *The model of etching of (hkl) planes in monocrystalline silicon*. J. Electrochem. Soc. 150, 2003, C391-C400.

[35] Baum, T. & Schiffrin, D. J., *Mechanistic aspects of anisotropic dissolution of materials etching of single-crystal silicon in alkaline solutions*. J. Chem. Soc., Faraday Trans. 94, 1998, 691-694.

[36] Hines, M. A., Chabal, Y. J., Harris, T. D., & Harris, A. L., *Measuring the structure of etched silicon surfaces with Raman spectroscopy*. J. Chem. Phys. 1994, 101, 8055-8072.

[37] Mills, D., Nahidi, M., & Kolasinski, K. W., *Stain Etching of Silicon Pillars and Macropores*. Phys. Status Solidi A 202, 2005, 1422-1426.

[38] Riedel, D., Hernández-Pozos, J. L., Kolasinski, K. W., & Palmer, R. E., *Arranged silicon conical spike structures from optical diffraction and ultrafast laser etching in halogen gas*. Appl. Phys. A 78,

2004, 381-385.

[39] Mills, D., Kreouzis, T., Sapelkin, A., Unal, B., Zyuzikov, N., & Kolasinski, K. W., *Surface texturing of Si, porous silicon and TiO_2 by laser ablation*. Appl. Surf. Sci. 253, 2007, 6575-6579.

[40] Kolasinski, K. W., *Porous Silicon Formation by Stain Etching*. In: *Handbook of Porous Silicon*, 2nd ed. (Ed.: L. T. Canham), Springer Verlag, Berlin, 2018, 1-21.

[41] Kolasinski, K. W., Gimbar, N. J., Yu, H., Aindow, M., Mäkilä, E., & Salonen, J., *Regenerative Electroless Etching of Silicon*. Angew. Chem., Int. Ed. Engl. 55, 2017, 624-627.